

Insight into differences in nanoindentation properties of bone

Naiara Rodriguez^{a*}, Michelle L. Oyen^b, Sandra J. Shefelbine^a

^a Department of Bioengineering, Imperial College London, London SW7 2AZ, UK

^b Department of Engineering, Cambridge University, Cambridge, CB2 1PZ, UK

*Corresponding author:

Naiara Rodriguez

Department of Bioengineering, 4.28/2

Imperial College London

London SW7 2AZ, UK

Email: nr211@imperial.ac.uk

Phone: +44 0787 350 9290

ABSTRACT

Nanoindentation provides the ideal framework to determine mechanical properties of bone at the tissue scale without being affected by the size, shape, and porosity of the bone. However, the values of tissue level mechanical properties vary significantly between studies. Since the differences in the bone sample, hydration state, and test parameters complicate direct comparisons across the various studies, these discrepancies in values cannot be compared directly. The objective of the current study is to evaluate and compare mechanical properties of the same bones using a broad range of testing parameters. Wild type C56BL6 mice tibiae were embedded following different processes and tested in dry and rehydrated conditions. Spherical and Berkovich indenter probes were used, and data analysis was considered within the elasto-plastic (Oliver-Pharr), viscoelastic and visco-elastic-plastic frameworks. The mean values of plane strain modulus varied significantly depending on the hydration state, probe geometry and analysis method. Indentations in dry bone analysed using a visco-elastic-plastic approach gave values of 34 GPa. After rehydrating the same bones and indenting them with a spherical tip and utilizing a viscoelastic analysis, the mean modulus value was 4 GPa, nearly an order of magnitude smaller. Results suggest that the hydration state, probe geometry and the limitations and assumptions of each analysis method influence significantly the measured mechanical properties. This is the first time that such a systematic study has been carried out and it has been concluded that the discrepancies in the mechanical properties of bone measured by nanoindentation found in the literature should not be attributed only to the differences on the bones themselves, but also to the testing and analysis protocols.

KEYWORDS: Nanoindentation, Bone, Visco-elastic-plastic, Viscoelastic, Oliver-Pharr, Hydration, probe geometry

NOMENCLATURE

A_C	contact area
C_i	creep function coefficients
E_R	reduced modulus
E'	plane strain modulus
f	viscous extent (G_∞/G_0)
G	shear modulus
G_0	zero-time shear modulus
G_∞	equilibrium shear modulus
G^I	incompressible shear modulus
h	indenter displacement
h_e	elastic displacement
h_{\max}	maximum displacement
h_p	plastic displacement
h_v	viscous displacement
H	hardness, resistance to plastic deformation
H_C	contact hardness, resistance to total deformation
P	indentation load
P_{\max}	peak load
S	stiffness
t	time
t_C	creep hold time
t_R	rise time
$\alpha_1, \alpha_2, \alpha_3$	dimensionless geometry constant
η_Q	indentation viscosity
ν	Poisson's ratio
T_i	viscous-elastic time constant

1 1. INTRODUCTION

2 Bone has a hierarchical structure in which the organization of its constituents at smaller
3 length scales determines the mechanical properties of the whole bone. At the tissue
4 level (sub-mm length scale) bone is composed of a matrix of mineralized collagen
5 fibrils and pores (vascular and lacunar). Unlike whole bone mechanical testing,
6 analysis of mechanical properties at the tissue scale is not affected by the size, shape,
7 and porosity of the bone, allowing for tissue level material properties to be determined.

8 Nanoindentation is a widely used technique to determine the mechanical properties of
9 bone at the tissue level (Guo and Goldstein 2000; Haque et al. 2003; Lewis and Nyman
10 2008; Oyen 2010; Rho et al. 1997; Zysset et al. 1999). In nanoindentation, a probe is
11 brought into contact with a surface, pushed into the material, and retracted, while the
12 load (P), displacement (h) and time (t) are recorded. Based on these P - h - t curves,
13 multiple models exist to extract mechanical properties depending on the deformation
14 modes of the indented material. Bone is heterogeneous, anisotropic, viscoelastic and
15 poroelastic and hence, various analytical and numerical models have been developed
16 and adapted to determine its tissue level mechanical properties such as elastic
17 modulus, hardness and effective (viscoelastic) viscosity (Isaksson et al. 2010; Mencik
18 et al. 2009; Olesiak et al. 2009; Oyen 2006a). Indentations on bone with sharp probes
19 result in plastic deformation; therefore, a viscoelastic-plastic (VEP) approach has been
20 used for Berkovich indentations (Olesiak et al. 2009; Oyen and Cook 2003). In
21 contrast, large spherical indenters may be used to maintain small indentation strains
22 thus preventing yielding and plastic deformation, allowing for viscoelastic (VE) analysis
23 (Oyen 2005, 2006a, 2007). The method that is built into most commercial indentation
24 systems is the Oliver – Pharr (OP) method (1992, 2004) to extract elastic-plastic
25 properties, neglecting any contribution from time-dependent deformation.

26 All three approaches, elasto-plastic, viscoelastic, and visco-elastic-plastic, have been
27 used to determine bone's mechanical response, but the values of the plane strain
28 modulus obtained from different studies vary significantly. In indentation of dry bone,
29 where OP analysis was used, Chang et al. (2011) measured a modulus of 30.8 ± 2.0
30 GPa using a Berkovich tip, while Bushby et al. (2004) found a modulus of 18.1 ± 2.4
31 GPa with a spherical tip. The viscoelastic approach in wet bone, using spherical
32 indentation, gave moduli as small as 2 GPa (Oyen et al. 2012). Olesiak et al. (2009)
33 obtained values of 24.78 ± 3.07 GPa in dry bone, utilizing sharp indentation and using
34 the VEP model. Since the differences in the sample preparation, hydration state, and
35 test parameters complicate direct comparisons across the various studies, these
36 discrepancies in values could not be compared directly.

37 The goal of the current study is to evaluate and compare mechanical properties of the
38 same bones using a wide range of testing and analysis methods. The bone is indented
39 both wet and dry, and after different embedding processes. Both spherical and
40 Berkovich indenter probes are utilized, and data analysis is considered within the OP,
41 VE and VEP frameworks. Thus, for the first time, direct comparisons of mechanical
42 properties of bone measured by nanoindentation after following different testing and
43 analysis protocols are available for analysis.

44 **2. MATERIALS AND METHODS**

45 Figure 1 shows an outline of the steps followed in the sample preparation and
46 nanoindentation test.

47 *2.1. Specimen Preparation*

48 Tibiae from four 9 week-old female C57BL/6 mice were harvested and cleaned of
49 surrounding soft tissue. One tibia from each mouse was cut transversally at the mid-
50 diaphysis using a low speed diamond saw (Isomet, Buehler GmbH, Germany). Half of
51 one tibia from each mouse (four halves) were fixed in 70% ethanol for 48 hours,

52 dehydrated in a series of increasing concentrations of ethanol (80, 90 and 100% for 24,
53 24 and 72 h respectively), and changed to a xylene solution (48 h).The bones were
54 then infiltrated in pure methyl methacrylate (MMA + α -azo-iso-butyronitrile, VRW, UK)
55 under vacuum for 24 hours. The MMA was changed for fresh MMA and infiltrated for
56 other 24 hours. The four half tibiae were kept in a vacuum chamber and they were let
57 to polymerize at room temperature for two weeks.

58 The rest of the tibiae (one whole and one half from each mouse) were kept frozen at -
59 20°C in phosphate buffered saline (PBS) gauze. Before embedding the tibiae were
60 thawed and dried in air for an hour, embedded in low viscosity epoxy resin (EPOTHIN;
61 Buehler, Lake Bluff, IL, USA), and allowed to cure at room temperature for 24 hours.
62 No vacuum chamber was used to minimize the infiltration of the epoxy in the bone. The
63 whole tibiae were also sectioned transversally at the mid-diaphysis in order to have 12
64 specimens (3 from each mouse) embedded in epoxy resin.

65 All cross-sections were polished using increasing grades of carbide papers (from P600
66 to P1200) and finally with diamond slurry of 3, 1, 0.25 and 0.05 μm particle size. The
67 samples were cleaned ultrasonically with distilled water between each polishing step.

68 *2.2. Nanoindentation*

69 Nanoindentation studies were conducted on the tibia mid-diaphyseal cross-sections
70 using the TI700 UBI (Hysitron, Minneapolis, MN, USA). A maximum load of 8 mN was
71 applied longitudinally at a constant loading rate of 0.8 mNs^{-1} following a holding time of
72 30 s (Figure 2). Nine indents were made in each specimen for each condition with a
73 minimum spacing of 10 μm between indents.

74 The indentation tests were first performed on the dry PMMA-infiltrated and epoxy-
75 embedded samples using a Berkovich diamond tip. Then the epoxy-embedded
76 specimens were rehydrated in distilled water overnight and a second set of
77 indentations with the same load protocol was carried out with the rehydrated samples.

78 Testing time for each sample was limited to 45 min to prevent sample drying. The
79 same dry-wet procedure was followed for testing with a 55 μm radius spherical tip. This
80 sphere size was chosen so that the contact areas were relatively small, for comparison
81 with the Berkovich results, but sufficiently large to avoid plasticity during indentation.

82 **3. DATA ANALYSIS**

83 *3.1. Models*

84 After completing the indentation tests following the trapezoidal loading (Figure 2), P-h-t
85 (Figure 3) plots were exported. Three different models (OP, VE and VEP) were used to
86 fit the data and to extract mechanical properties of the material.

87

88 *3.1.1. Oliver-Pharr (OP)*

89 In the commonly used Oliver-Pharr approach (Oliver and Pharr 1992, 2004) the elastic
90 modulus is calculated from the unloading curve based on the assumption that the
91 unloading response is purely elastic. Due to the time-dependent behavior of bone, the
92 unloading is viscoelastic; nevertheless, an attempt is made to limit the contribution of
93 viscoelasticity by introducing 30s creep hold at peak load (Briscoe et al. 1998;
94 Chudoba and Richter 2001; Feng and Ngan 2002).

95 In the OP method, the stiffness at peak load (S) is calculated as the slope of the
96 unloading curve. In the current study, 80% of the unloading curve has been used to
97 obtain the slope. The contact area (A_c) is the projected area obtained via a calibration
98 function. These two parameters are used to compute the reduced modulus:

$$E_R = \frac{S\sqrt{\pi}}{2\sqrt{A_c}} \quad [1]$$

99 The reduced modulus is a combination of indenter and sample material properties.
 100 However, since bone is far less stiff than the diamond tip with ($E < 30\text{GPa}$) the reduced
 101 modulus can be considered as the plane strain modulus ($E_R \sim E'$) (Olesiak et al. 2009).
 102 The contact hardness or the mean supported contact stress is the peak load divided by
 103 the contact area.

$$H_c = P_{max}/A_c \quad [2]$$

104

105 3.1.2. Viscoelastic Analysis (VE)

106 Negligible plastic deformation occurs with spherical indenter tips provided that the
 107 indentation strain is smaller than the yield strain, allowing for the use of viscoelastic
 108 analysis (Oyen 2005, 2006a, 2007). In this method, a linear viscoelastic response and
 109 a non-decreasing contact area are assumed. For spherical indentations, the creep
 110 period (h-t during the holding time) is fitted by a generalized standard linear solid model
 111 (Figure 3.b):

$$h^{3/2}(t) = \frac{3}{8\sqrt{R}} P_{max} \left[C_0 - \sum_i^2 C_i \exp(-t/\tau_i) RCF_i \right] \quad [3]$$

112 Where the radius of the sphere, R , and the peak load, P_{max} , are test parameters; and
 113 C_0 , C_i and τ_i are the fitting parameters. C_0 and C_i represent the creep coefficients and
 114 $\tau_i(\eta_i/E_i)$ are material time constants. In this study, two Kelvin-Voigt bodies and therefore
 115 two time constants (τ_1, τ_2) have been used to represent bone creep. The dimensionless
 116 ramp correction factor, RCF_i , accounts for the fact that the loading is not instantaneous
 117 (rising time, $t_R > 0$) and it is given by (Oyen 2007):

$$RCF_i = \frac{\tau_i}{t_R} [\exp(t_R/\tau_i) - 1] \quad [4]$$

118 From the obtained creep coefficients, the instantaneous G_0 and long-time G_∞ shear
119 modulus for the incompressible ($\nu = 0.5$) case can be computed as:

$$G_0 = \frac{1}{2(C_0 - \sum C_i)} \quad [5]$$

$$G_\infty = \frac{1}{2C_0} \quad [6]$$

120 The ratio of these two extremes $f = G_\infty / G_0$ gives an idea of the extent of the time-
121 dependent deformation, where $f = 1$ signifies a perfectly elastic material and $f = 0$ a
122 perfectly viscous material.

123 Since in bone $\nu = 0.3$, the calculated incompressible ($\nu = 0.5$) zero-time shear modulus
124 G^I must be translated to G^V via (Oyen 2005):

$$G^V = 2G^I(1 - \nu) \quad [7]$$

125 The plane strain modulus is obtained from the incompressible instantaneous shear
126 modulus (Bembey 2006):

$$E' = \frac{2G}{1 - \nu} \quad [8]$$

127 3.1.3. Viscoelastic-Plastic Analysis (VEP)

128 Sharp indenter tips, such as a Berkovich pyramid, result in plastic deformations and a
129 viscoelastic-plastic analysis is appropriate (Olesiak et al. 2009). This method combines
130 viscous, elastic and plastic quadratic elements in series (Figure 4.a) to model the full
131 response of time-dependent materials (Oyen and Cook 2003). Using a trapezoidal
132 loading function shown in Figure 1, the full VEP displacement-time (h - t) response is
133 defined by equations 9-11 (Olesiak et al. 2009): the loading has a viscous-elastic-
134 plastic behaviour (h^{LOAD}), the holding period is defined by a viscous response (h^{CREEP})
135 and the unloading is viscoelastic (h^{UNLOAD}).

$$h^{LOAD}(t) = (kt)^{1/2} \left(\frac{2t}{3(\alpha_3 \eta_Q)^{1/2}} + \frac{1}{(\alpha_2 E')^{1/2}} + \frac{1}{(\alpha_1 H)^{1/2}} \right) \quad t < t_R \quad [9]$$

$$h^{CREEP}(t) = \frac{(kt_R)^{1/2}}{(\alpha_3 \eta_Q)^{1/2}} (t - t_R) + h^{LOAD}(t_R) \quad t_R < t < t_R + t_c \quad [10]$$

$$h^{UNLOAD}(t) = (kt)^{1/2} \left(\frac{t_R^{3/2} - (2t_R + t_c - t)^{3/2}}{3/2(\alpha_3 \eta_Q)^{1/2}} + \frac{(2t_R + t_c - t)^{1/2} - t_R^{1/2}}{(\alpha_2 E')^{1/2}} \right) + h^{CREEP}(t_R + t_c) \quad t > t_R + t_c \quad [11]$$

136

137 The dimensionless geometric constants for a perfect Berkovich tip are $\alpha_1 = 24.5$, $\alpha_2 = \alpha_3$
 138 = 4.4 (Oyen and Cook 2003); t_R , t_c stand for the rising time and holding time
 139 respectively; k is the loading rate ($k = P_{max}/t_R$). Fitting the displacement time (h - t) curve
 140 to the full VEP solution allows for the direct extraction of the indentation viscosity (η_Q),
 141 plane strain modulus (E') and hardness (H , resistance to plastic deformation). In
 142 addition, the contact hardness (H_c , resistance to all components of deformation) can be
 143 calculated for comparison purposes with the Oliver-Pharr hardness (Oyen 2006b).

$$H_c = \frac{P_{max}}{\alpha_1 (h_v + h_e + h_p)^2} = \frac{1}{\alpha_1 \left((2t_R/3)(\alpha_3 \eta_Q)^{-1/2} + (\alpha_2 E')^{-1/2} + (\alpha_1 H)^{-1/2} \right)^2} \quad [12]$$

144

145 In the VEP model a linear creep rate is assumed for the entire hold period. However,
 146 this is only an approximation, and therefore only the steady-state creep was used to
 147 estimate the viscosity term:

$$h^{CREEP}(t) = \frac{(P_{max})^{1/2}}{(\alpha_3 \eta_Q)^{1/2}} (t - t_1) + h(t_1) \quad [13]$$

148

149 where t_1 is defined as $t_1 = t_R + t_c/6$ to only consider the last 5/6 of the holding period
 150 and obtain a better fit of the curve.

151 The nonlinear least-square curve-fit function in MATLAB (Mathworks, Natick, MA) was
 152 used to extract the mechanical properties from this 3-step process: i) η_Q was calculated
 153 by fitting the holding period; ii) knowing the indentation viscosity, E' was obtained from
 154 the unloading curve; ii) finally, while these two parameters were held constant, the
 155 loading curve was used to compute H . The viscous time constant was defined as $\tau_Q =$
 156 $(\eta_Q/E')^{1/2}$ and represents the characteristic time scale of the material associated with
 157 the viscous-elastic-plastic response to indentation.

158 3.2. Deformation partitioning

159 From the OP model, the plastic (h_{p_OP}) deformation could be approximated to the
 160 displacement at zero load at the end of the test. The elastic deformation (h_{e_OP}) could
 161 be defined as the difference between the maximum and final deformation.

$$h_{p_OP} \approx h(t_{max}) = h_{final} \quad [14]$$

$$h_{e_OP} = h_{max} - h_{p_OP} \quad [15]$$

162 In sharp indentations, the VEP model allows for the partitioning of the indentation
 163 response into independent elastic (h_{e_VEP}), plastic (h_{p_VEP}) and viscous (h_{v_VEP})
 164 deformation components (Ferguson 2009).

$$h_{max} = h_{e_VEP} + h_{p_VEP} + h_{v_VEP} \quad [16]$$

165 Where each of the deformations can be defined as:

$$h_{e_VEP} = \sqrt{\frac{P_{max}}{\alpha_2 E'}} \quad [17]$$

$$h_{p_VEP} = \sqrt{\frac{P_{max}}{\alpha_1 H}} \quad [18]$$

$$h_{v_VEP} = \sqrt{\frac{P_{max}}{\alpha_3 \eta_Q}} \left(\frac{2}{3} t_R + t_C \right) \quad [19]$$

166 For spherical indentations with large radius, only elastic and viscous deformations are
 167 present. In the VE analysis, the displacement is defined as a function of the shear
 168 modulus.

$$h^{3/2}(t) = \frac{3}{16\sqrt{R}} \frac{P_{max}}{G} \quad [20]$$

169 Hence, the displacement associated with the equilibrium modulus is the elastic
 170 displacement (h_{e_VE}), while the difference between this and the displacement
 171 associated with the instantaneous modulus represents the viscous deformation (h_{v_VE}).

$$h_{e_VE} = \left(\frac{3}{16\sqrt{R}} \frac{P_{max}}{G_\infty} \right)^{2/3} \quad [21]$$

$$h_{v_VE} = h_{e_VE} - \left(\frac{3}{16\sqrt{R}} \frac{P_{max}}{G_0} \right)^{2/3} \quad [22]$$

172

173 3.3. Statistical evaluation

174 Mean values and standard deviations of the mechanical properties of each specimen
 175 were computed. Normality tests were carried out between these means using Shapiro-
 176 Wilk test. Dependent t-test was used to compare normally distributed data sets;
 177 Wilcoxon signed-rank test was used for non-parametric data. A difference was
 178 considered significant when $p < .05$. Statistical analysis was performed using SPSS (v.
 179 20, SPSS Inc., Chicago, IL).

180 4. RESULTS

181 Table 1 summarizes the mean values of the mechanical properties obtained from this
 182 study. From the VEP analysis, the plane strain modulus (E'), hardness (H), contact

183 hardness (H_c), indentation viscosity (η_Q) and time constant (τ_1) are measured, OP
184 method gives the reduced modulus (E_R , which in this case is equal to E') and the
185 contact hardness (H_c), while from the VE approach the plane strain modulus (E') and
186 the extent of viscosity (f) are calculated together with the time constants (τ_1, τ_2).

187 The mean values of plane strain modulus, which is one parameter comparable across
188 all models, vary significantly depending on the test method, as shown in Figure 5.

189 Berkovich indentations on epoxy-embedded dry bones analyzed by VEP gave a mean
190 plane strain modulus of 33.7 GPa; while after rehydrating the same bones and
191 indenting them with a spherical tip and utilizing a VE analysis, the mean modulus value
192 was nearly an order of magnitude smaller, at 4.1 GPa.

193 *4.1. Embedding medium*

194 No significant differences were found between the plane strain modulus and viscosity
195 values of dry epoxy-embedded and PMMA-infiltrated samples across the models.

196 However, the VEP model showed that the hardness was larger for PMMA-infiltrated
197 samples ($H_{\text{PMMA}} = 2.57 \pm 0.40$ GPa) than for epoxy embedded ones ($H_{\text{epoxy}} = 1.91 \pm$
198 0.56 GPa).

199 *4.2. Hydration state*

200 Plane strain modulus was significantly greater in dry specimens than in rehydrated
201 specimens in all the cases. The VEP model showed that the hardness and the viscosity
202 term were also significantly higher in dry specimens ($H_{\text{dry}} = 1.91 \pm 0.56$ GPa, $\eta_{Q, \text{dry}} =$
203 $2.53 \pm 1.62 \times 10^{15}$ Pa s²) than in their wet counterparts ($H_{\text{wet}} = 0.47 \pm 0.11$ GPa, $\eta_{Q, \text{wet}} =$
204 $0.50 \pm 0.28 \times 10^{15}$ Pa s²).

205 *4.3. Deformation partitioning*

206 The elastic, plastic and viscous deformations and deformation fractions for each
207 condition are summarized in Figure 6. Both in Berkovich and spherical indentations, the
208 total deformation increases from dry to rehydrated conditions. However the deformation

209 partitioning depends on the method used to analyze the same data. Similar
210 deformation trends are found in VEP and OP approaches: elastic deformation does not
211 vary significantly when rehydrating the samples, while plastic and viscous deformations
212 increase; unlike the viscous deformation fraction, elastic and plastic fractions vary
213 significantly from dry to rehydrated conditions. The VE model shows the highest elastic
214 and viscous deformations, showing a significant increase in both deformations from dry
215 to wet conditions. In contrast, the values of elastic and viscous fractions analyzed by
216 VE do not depend on the hydration state.

217 **5. DISCUSSION**

218 In this study, systematic investigations of the effect of a wide range of indentation
219 testing methodological options were considered for indentation of the same bone
220 samples. The results show that the measured mechanical properties depend on the
221 hydration state of the samples, the probe geometry and the model used to analyze the
222 data. As shown in Figure 7, the plane strain modulus values obtained in this study are
223 comparable to the wide range of values found in literature. In sharp indentations,
224 Chang et al. (2011) measured plane strain modulus of 31 GPa for B6 mice femur
225 embedded in epoxy. Lopez-Franco et al. (2011) found modulus of 22 GPa in NTG mice
226 femur submerged in water. Bushby et al. (2004) had modulus of 18 GPa for equine
227 bone embedded in PMMA indented using a spherical tip. Spherical indentations on fully
228 rehydrated equine bone gave modulus as small as 2 GPa (Oyen et al. 2012) after
229 analyzing the data using a viscoelastic approach. Until now, these discrepancies in
230 values were considered to be mainly the result of the differences on the bones
231 themselves. However, this study demonstrates that different methods give different
232 results even on the same bone.

233

234

235 *5.1. Wet vs dry bone*

236 As shown in Fig. 5, plane strain modulus was significantly higher in dry specimens than
237 in rehydrated specimens in all the cases. This tendency is in accordance with literature
238 (Bushby 2004; Hoffler 2005; Bembey 2006a, 2006b). The deformation partitioning
239 (Figure 6.a) showed that in all the cases the total deformation is bigger when
240 rehydrating the bone. It must be noted that the wet samples considered here were not
241 immersed in fluid while testing, and therefore the differences in values of fully
242 rehydrated samples might be larger than the ones currently measured. All the methods
243 trend in the same direction showing the capability of nanoindentation to capture
244 differences in hydration states.

245 *5.2. Probe geometry*

246 One of the most important experimental selections is that of probe geometry, which has
247 been shown to influence the indentation response. Berkovich indentors have a sharp
248 tip and the transition from elastic to plastic behavior happens almost instantaneously,
249 indicated by the deformation partitioning which shows a plastic deformation fraction of
250 60-80% (Figure 6.b). In contrast, spherical tips allow extended elastic to plastic
251 transition, which can be easily detectable by plotting P-h curves in logarithmic scale
252 (Oyen, 2011). Figure 8 shows that in the beginning the load is proportional to the
253 displacement instead of following the $P \sim h^{3/2}$ elastic law. A curve parallel to the P-h line
254 is associated with plastic behavior of the material. However, from the mechanics point
255 of view, the response cannot move from a plastic regime to an elastic one. This means
256 that the indenter tip detected the contact surface too early and this induced a first
257 regime where the load and displacement were proportional. Hence, the measured
258 contact displacement is overestimated and so is the contact area. This might cause an
259 underestimation in the plane strain modulus value (Zhang et al. 2008). In the current
260 study, the data was rejected if the initial roughness curve exceeded 5% of the
261 maximum load. Nevertheless, roughness is the likely one cause of discrepancies

262 between the Oliver-Pharr results for bone tested in the same condition—wet or dry—
263 with the two different tips.

264 Figure 6.b shows the viscous, plastic and elastic deformation fractions – h_v/h_{max} , h_p/h_{max}
265 and h_e/h_{max} - for both probe geometries. In Berkovich indentations the viscous
266 deformation fraction is less than 10%. Hence, even if Oliver-Pharr method does not
267 capture time-dependent deformation, the deformation fractions for VEP and OP are
268 similar. On the other hand, in spherical indentations the viscous deformation is about
269 25% of the total deformation. The P-h curves in logarithmic scale (Figure 8) have
270 shown that there was no plasticity induced in spherical indentations but the deformation
271 partitioning in the OP case shows that the plastic deformation is dominant. This reflects
272 the limitations of the Oliver-Pharr method to measure mechanical properties of time-
273 dependent materials.

274 *5.3. Embedded versus infiltrated*

275 The embedding protocol did not result in significant differences between the plane
276 strain modulus and viscosity values across the models. This demonstrates that
277 nanoindentation measures local properties of bone. However, the VEP model showed
278 that the hardness was higher for PMMA-infiltrated samples. Unlike in epoxy samples, in
279 PMMA samples, a vacuum chamber was used to infiltrate the resin into the bone
280 pores, which could contribute to an increase in hardness.

281 *5.4. Analysis method: assumptions and limitations*

282 Bone is heterogeneous, anisotropic, viscoelastic, and poroelastic, with a viscoelastic
283 unloading curve (Oyen and Cook 2003). OP analysis cannot capture the viscous
284 behavior of bone. The VEP is a single time constant model and its prediction capability
285 is limited when indenting a hierarchical material with different time scales such as bone
286 (Wang and Lloyd 2010). The VE model with two time constants gives a better
287 approximation of the creep hold period than the VEP model. The time constants give

288 information about the time scales of deformation in the material relative to the time
289 frame of the experiment.

290 All three models for data analysis here are based on the same fundamental elastic
291 contact mechanics for indentation (Sneddon 1965). The extension of elastic to VE (Lee
292 and Radok 1960) is the approach containing the most direct adaptation of elastic
293 contact mechanics, and that containing the fewest simplifying assumptions. Once
294 plastic deformation is included, the picture gets more complicated. While Oliver-Pharr
295 has been shown to be accurate for stiff materials, it overestimates modulus values for
296 polymeric materials (Ngan et al. 2005; Tranchida et al. 2007), in part because of the
297 time-dependent deformation in polymers (including bone). The VEP model used here
298 has the most *a priori* assumptions. VEP assumes that the viscous, plastic and elastic
299 deformations are in series and that the creep is linear, which is too simple to capture
300 the more complex, multiple time constant behavior observed in bone. This results in
301 modulus values that are the greatest when compared with either a viscoelastic or OP
302 approach. A tendency towards modulus overestimation was observed when this model
303 was used for characterization of polymers as well (Oyen and Cook 2003). Therefore,
304 VEP is useful for comparison of groups within studies, but further development of this
305 model is required before quantitative material properties can be determined.

306 Each of the analytical models considered here is fit to different parts of the indentation
307 load-displacement-time response. The most direct differences observed here were for
308 spherical indentation using Oliver-Pharr, which is a fit only to the unloading data, and
309 VE, which is a fit only to the load-hold data. The reasons for the large discrepancy
310 between the obtained modulus values in these two cases certainly requires further
311 detailed study in the future, but the most likely explanation is the failure of OP to
312 account for viscoelastic deformation during unloading. This study provides the most
313 direct evidence yet of the extent of this effect in materials with time-dependent
314 mechanical behavior. While many studies have advocated for a hold period at peak

315 load to “exhaust” viscoelastic deformation and minimize the effect during unloading, the
316 results here demonstrate that this approach does not provide reliable quantitative data
317 on bone nanoindentation. Similar results were achieved by Oyen and Ko (2007) after
318 using the VEP model to generate two load-displacement curves for plane strain
319 modulus that differed by a factor of 2 and resulted in equivalent unloading stiffness
320 which would lead to a difference in modulus of only a factor of 1.2.

321 Summarizing, the OP method could be used for a fast identification of relative
322 differences in the elastic modulus between samples. The VEP model provides an
323 estimation of the elastic, plastic and viscous contributions to the bone material behavior
324 in sharp indentations. And the VE approach can be used to analyze the creep behavior
325 of bone when there is no plasticity induced.

326 **6. CONCLUSIONS**

327 This is the first time that the same bones have been tested systematically following
328 different testing and analysis options. This study demonstrates that the tissue level
329 mechanical properties of bone measured by nanoindentation depend not only on the
330 sample itself, but also on the hydration state, probe geometry and data analysis
331 method. This is why it is complicated to compare values from different studies and care
332 must be taken when choosing the experimental and analytical options. The current
333 work shows that nanoindentation is capable of capturing trends in the mechanical
334 properties. It provides the framework to compare tissue level mechanical properties of
335 different type of bones, such as bones of different ages or pathologies.

336 **ACKNOWLEDGEMENTS**

337 This study has been funded by BBSR and the Basque Government predoctoral
338 fellowship.

REFERENCES

1. Bembey, A.K., Oyen, M.L., Bushby, A.J., Boyde, A., 2006a. Viscoelastic properties of bone as a function of hydration state determined by nanoindentation. *Philosophical Magazine* 86, 5691–5703.
2. Bembey, A. k., Bushby, A. j., Boyde, A., Ferguson, V. I., Oyen, M. I., 2006b. Hydration effects on the micro-mechanical properties of bone. *Journal of Materials Research* 21, 1962–1968.
3. Briscoe, B.J., Fiori, L., Pelillo, E., 1998. Nano-indentation of polymeric surfaces. *Journal of Physics D: Applied Physics* 31, 2395–2405.
4. Bushby, A. j., Ferguson, V. I., Boyde, A., 2004. Nanoindentation of Bone: Comparison of Specimens Tested in Liquid and Embedded in Polymethylmethacrylate. *Journal of Materials Research* 19, 249–259.
5. Chang, Y.-T., Chen, C.-M., Tu, M.-Y., Chen, H.-L., Chang, S.-Y., Tsai, T.-C., Wang, Y.-T., Hsiao, H.-L., 2011. Effects of osteoporosis and nutrition supplements on structures and nanomechanical properties of bone tissue. *Journal of the Mechanical Behavior of Biomedical Materials* 4, 1412–1420.
6. Chudoba, T., Richter, F., 2001. Investigation of creep behaviour under load during indentation experiments and its influence on hardness and modulus results. *Surface and Coatings Technology* 148, 191–198.
7. Feng, G., Ngan, A.H.W., 2002. Effects of Creep and Thermal Drift on Modulus Measurement Using Depth-sensing Indentation. *Journal of Materials Research* 17, 660–668.
8. Ferguson V.L., 2009. Deformation partitioning provides insight into elastic, plastic, and viscous contributions to bone material behavior. *Journal of the Mechanical Behavior of Biomedical Materials* 2, 364–374.
9. Guo, X.E., Goldstein, S.A., 2000. Vertebral trabecular bone microscopic tissue elastic modulus and hardness do not change in ovariectomized rats. *J. Orthop. Res.* 18, 333–336.
10. Haque, F., 2003. Application of Nanoindentation Development of Biomedical to Materials. *Surface Engineering* 19, 255–268.
11. Hoffler, C.E., Guo, X.E., Zysset, P.K., Goldstein, S.A., 2005. An Application of Nanoindentation Technique to Measure Bone Tissue Lamellae Properties. *J. Biomech. Eng.* 127, 1046–1053.
12. Isaksson, H., Nagao, S., Małkiewicz, M., Julkunen, P., Nowak, R., Jurvelin, J.S., 2010. Precision of nanoindentation protocols for measurement of viscoelasticity in cortical and trabecular bone. *Journal of Biomechanics* 43, 2410–2417.
13. Lee, E.H., Radok, J.R.M., 1960. The Contact Problem for Viscoelastic Bodies. *Journal of Applied Mechanics* 27, 438.

14. Lewis, G., Nyman, J.S., 2008. The use of nanoindentation for characterizing the properties of mineralized hard tissues: State-of-the art review. *Journal of Biomedical Materials Research Part B: Applied Biomaterials* 87B, 286–301.
15. Lopez Franco, G.E., Blank, R.D., Akhter, M.P., 2011. Intrinsic material properties of cortical bone. *J. Bone Miner. Metab.* 29, 31–36.
16. Menčík, J., He, L.H., Swain, M.V., 2009. Determination of viscoelastic–plastic material parameters of biomaterials by instrumented indentation. *Journal of the Mechanical Behavior of Biomedical Materials* 2, 318–325.
17. Ngan, A.H.W., Wang, H.T., Tang, B., Sze, K.Y., 2005. Correcting power-law viscoelastic effects in elastic modulus measurement using depth-sensing indentation. *International Journal of Solids and Structures* 42, 1831–1846.
18. Olesiak, S.E., Oyen, M.L., Ferguson, V.L., 2009. Viscous-elastic-plastic behavior of bone using Berkovich nanoindentation. *Mechanics of Time-Dependent Materials* 14, 111–124.
19. Oliver, W. c., Pharr, G. m., 1992. An improved technique for determining hardness and elastic modulus using load and displacement sensing indentation experiments. *Journal of Materials Research* 7, 1564–1583.
20. Oliver, W. c., Pharr, G. m., 2004. Measurement of hardness and elastic modulus by instrumented indentation: Advances in understanding and refinements to methodology. *Journal of Materials Research* 19, 3–20.
21. Oyen, M.L., Cook, R.F., 2003. Load–displacement Behavior During Sharp Indentation of Viscous–elastic–plastic Materials. *Journal of Materials Research* 18, 139–150.
22. Oyen, M.L., 2005. Spherical indentation creep following ramp loading. *Journal of Materials Research* 20, 2094–2100.
23. Oyen, M.L., 2006a. Analytical techniques for indentation of viscoelastic materials. *Philosophical Magazine* 86, 5625–5641.
24. Oyen, M.L., 2006b. Nanoindentation hardness of mineralized tissues. *J Biomech* 39, 2699–2702.
25. Oyen, M.L., 2007. Sensitivity of polymer nanoindentation creep measurements to experimental variables. *Acta Materialia* 55, 3633–3639.
26. Oyen, M.L., Ko, C.-C., 2007. Examination of local variations in viscous, elastic, and plastic indentation responses in healing bone. *J Mater Sci Mater Med* 18, 623–628.
27. Oyen, M.L., 2010. *Handbook of Nanoindentation: With Biological Applications*. Pan Stanford Publishing.
28. Oyen, M.L., 2011. *Nanoindentation of Biological and Biomimetic Materials. Experimental Techniques*.

29. Oyen, M.L., Shean, T.A.V., Strange, D.G.T., Galli, M., 2012. Size Effects in Indentation of Hydrated Biological Tissues. *Journal of Materials Research* 27, 245–255.
30. Rho, J.Y., Tsui, T.Y., Pharr, G.M., 1997. Elastic properties of human cortical and trabecular lamellar bone measured by nanoindentation. *Biomaterials* 18, 1325–1330.
31. Sneddon, I.N., 1965. The relation between load and penetration in the axisymmetric boussinesq problem for a punch of arbitrary profile. *International Journal of Engineering Science* 3, 47–57.
32. Tranchida, D., Piccarolo, S., Loos, J., Alexeev, A., 2007. Mechanical Characterization of Polymers on a Nanometer Scale through Nanoindentation. A Study on Pile-up and Viscoelasticity. *Macromolecules* 40, 1259–1267.
33. Wang, Y., Lloyd, I.K., 2010. Time-dependent nanoindentation behavior of high elastic modulus dental resin composites. *Journal of Materials Research* 25, 529–536.
34. Zhang, J., Niebur, G.L., Ovaert, T.C., 2008. Mechanical property determination of bone through nano- and micro-indentation testing and finite element simulation. *J Biomech* 41, 267–275.
35. Zysset, P.K., Edward Guo, X., Edward Hoffler, C., Moore, K.E., Goldstein, S.A., 1999. Elastic modulus and hardness of cortical and trabecular bone lamellae measured by nanoindentation in the human femur. *Journal of Biomechanics* 32, 1005–1012.

FIGURE CAPTIONS

Figure 1:

Outline of the methods. Tibiae of four B6 mice were harvested and cut in half. One of the halves was dehydrated in ethanol and infiltrated with PMMA using vacuum. The other three halves were dried in air and embedded in epoxy resin. The PMMA samples were tested only in dry conditions and the epoxy ones in dry and wet conditions. For each condition, nine indents were made both with a Berkovich indenter and a sphere.

Figure 2:

Trapezoidal load function. Loading to the peak load ($P_{max} = 8 \text{ mN}$) during rise time ($t_R = 10 \text{ s}$) with a creep hold ($t_c = 30 \text{ s}$) before unloading. Same loading and unloading rate ($k = P_{max}/t_R$).

Figure 3:

Load-displacement (a) and displacement-time (b) plots obtained after applying the trapezoidal loading protocol in Figure 2 on a rehydrated sample using a Berkovich indenter probe.

Figure 4:

Rheological model for (a) VEP on loading (adapted from Oyen and Cook 2003); and (b) VE during creep hold.

Figure 5:

Mean plane strain modulus and standard deviations for Berkovich indentations analyzed by VEP and OP and spherical indentations modeled with OP and VE in dry and rehydrated conditions.

Figure 6:

Viscous h_v , plastic h_p , and elastic h_e mean deformations (a) and mean deformation fractions (b) of Berkovich and spherical indentations in dry and rehydrated conditions.

Figure 7:

Comparison of the mean plane strain modulus of the current study (outlined) with other studies on dry and wet bone indented using Berkovich and spherical indenter probes. The analysis method used in each study is specified (OP, VE or VEP). The values obtained in this study for the same bones are comparable with the wide range found in the literature for different animal bones.

Figure 8:

Logarithmic curve of P-h data for a spherical indent on dry bone embedded in epoxy together with P~h (plastic behavior) and P~h^{3/2} (elastic behavior) curves.

TABLES

		Berkovich		Sphere (55µm)	
		VEP	OP	VE	OP
Dry pmma	E' [GPa]	36.4 ± 9.0	22.9 ± 3.7	7.2 ± 2.6	15.4 ± 3.7
	H [GPa]	2.57 ± 0.40			
	Hc [GPa]	0.93 ± 0.06	0.93 ± 0.07		0.17 ± 0.05
	η_Q (x 10 ¹⁵) [Pa s ²]	2.96 ± 1.86			
	f = G _∞ /G ₀			0.63 ± 0.04	
	τ_1, τ_2 [s]	277.2 ± 64.7		2.0 ± 0.8 19.6 ± 14.6	
Dry epoxy	E' [GPa]	33.7 ± 6.4	20.1 ± 3.9	6.6 ± 2.0	11.6 ± 1.7
	H [GPa]	1.91 ± 0.56			
	Hc [GPa]	0.75 ± 0.16	0.74 ± 0.19		0.15 ± 0.05
	η_Q (x 10 ¹⁵) [Pa s ²]	2.53 ± 1.62			
	f = G _∞ /G ₀			0.54 ± 0.13	
	τ_1, τ_2 [s]	252.0 ± 73.4		2.0 ± 0.7 18.8 ± 11.5	
Wet epoxy	E' [GPa]	27.5 ± 6.5	11.5 ± 2.0	4.1 ± 1.4	9.2 ± 2.4
	H [GPa]	0.47 ± 0.11			
	Hc [GPa]	0.26 ± 0.04	0.23 ± 0.03		0.10 ± 0.04
	η_Q (x 10 ¹⁵) [Pa s ²]	0.50 ± 0.28			
	f = G _∞ /G ₀			0.51 ± 0.08	
	τ_1, τ_2 [s]	133.3 ± 39 .0		2.0 ± 0.6 17.3 ± 9.0	

Table 1: Summary of means and standard deviations of tissue mechanical properties according to the probe geometry and data analysis method. E' is plane strain modulus; H is hardness (resistance to plastic deformation); Hc is contact hardness (resistance to deformation); η_Q is indentation viscosity; f represents the elastic fraction (viscous, 0 ≤ f ≤ 1, elastic); and τ_1, τ_2 are viscoelastic time constants (one time constant for VEP and two for VE).

339

340

341

342

343

344

345

346

347

348 **FIGURES**

349 Figure 1:

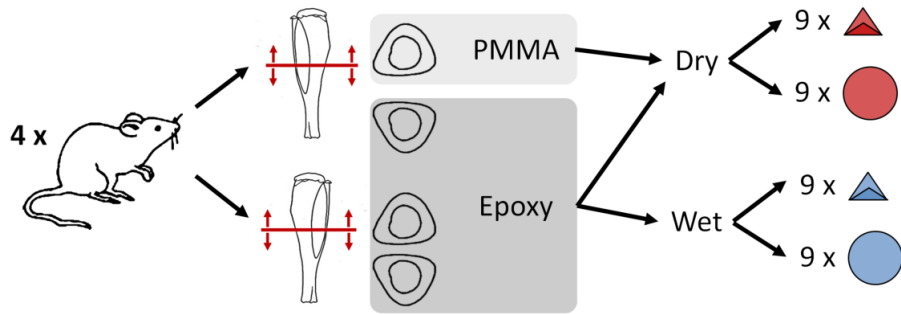


Figure 2:

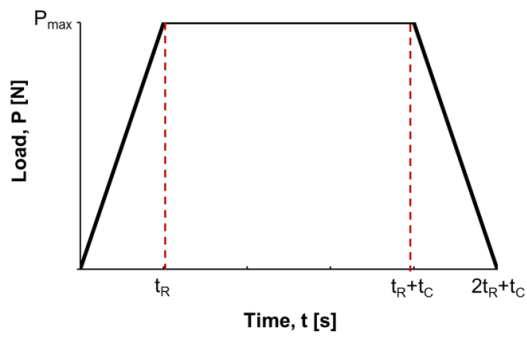


Figure 3:

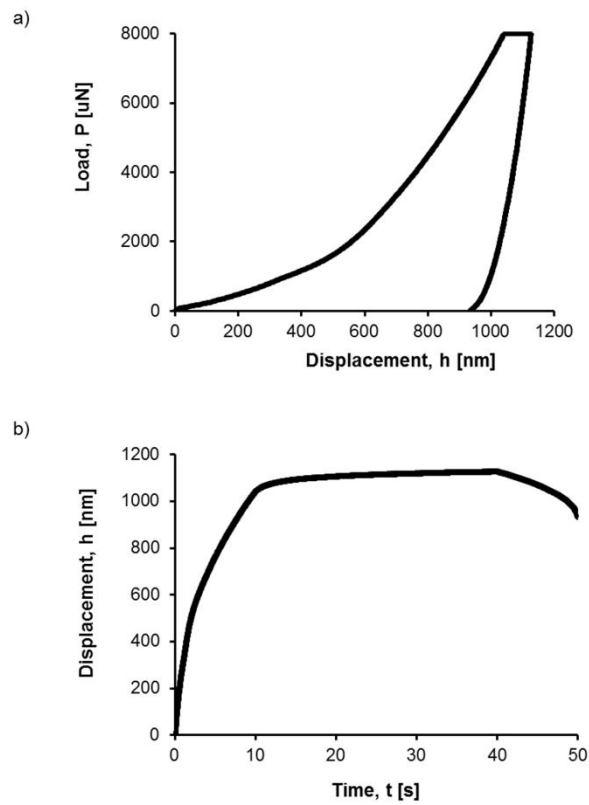


Figure 4:

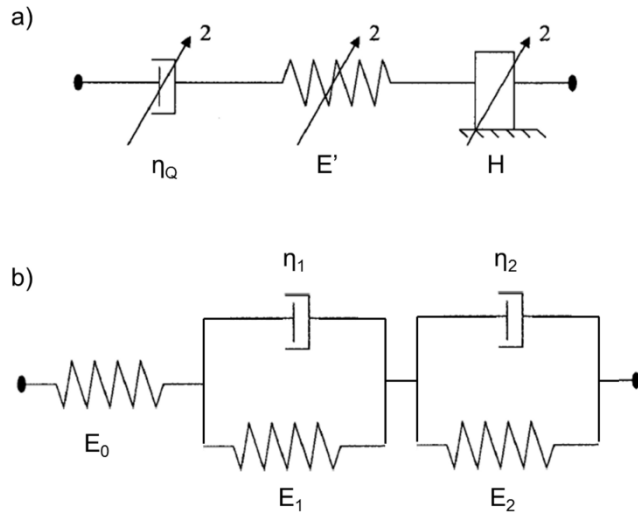


Figure 5:

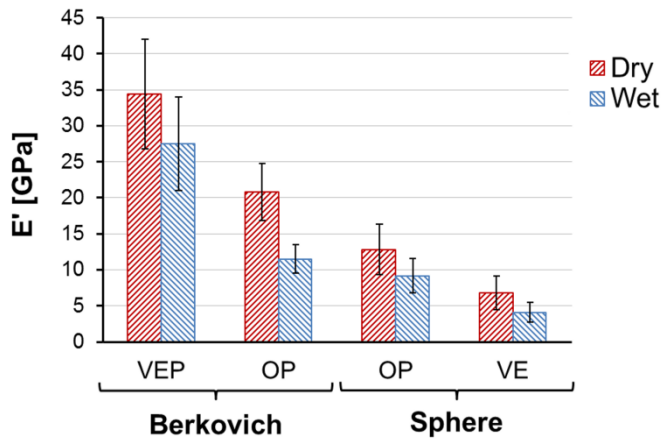


Figure 6:

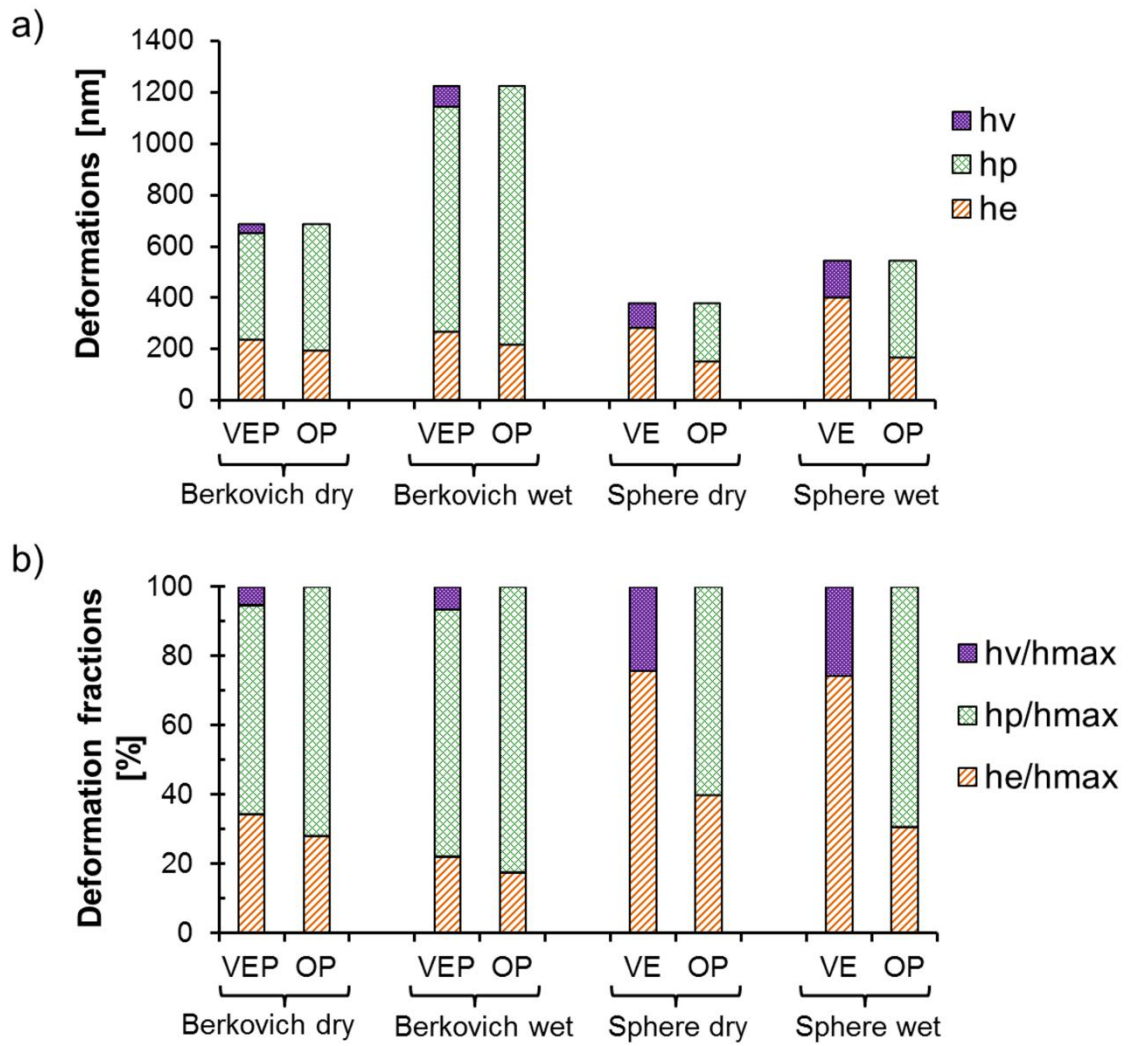


Figure 7:

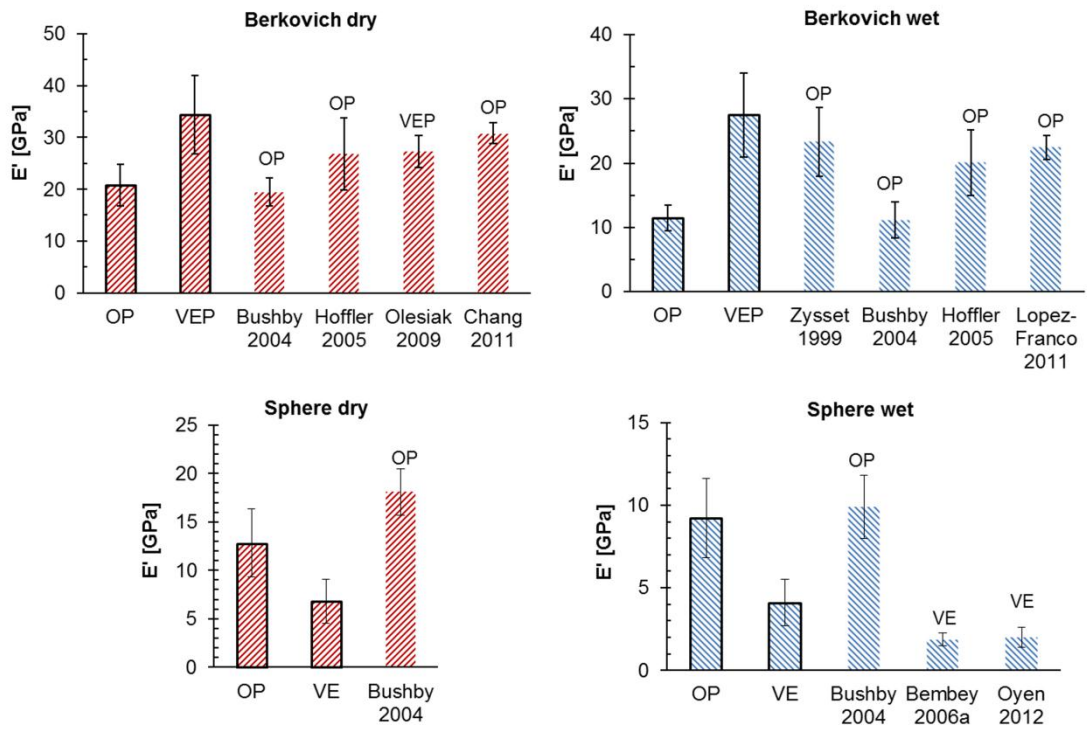


Figure 8:

